

Energy and Electron Transfer Dynamics within a Series of Perylene Diimide/Cyclophane Systems

Seán T. J. Ryan,[†] Ryan M. Young,^{‡,¶} James J. Henkelis,[‡] Nema Hafezi,[‡] Nicolaas A. Vermeulen,[‡] Andreas Hennig,[§] Edward J. Dale,[‡] Yilei Wu,^{‡,¶} Matthew D. Krzyaniak,^{‡,¶} Athan Fox,[†] Werner M. Nau,[§] Michael R. Wasielewski,^{‡,¶} J. Fraser Stoddart,[‡] and Oren A. Scherman^{*,†}

[†]Melville Laboratory for Polymer Synthesis, Department of Chemistry, University of Cambridge, Lensfield Road, Cambridge, CB2 1EW, U.K.

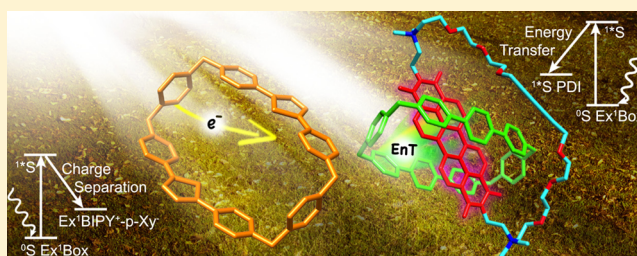
[‡]Department of Chemistry, Northwestern University, Evanston, Illinois 60208-3113, United States

[¶]Argonne-Northwestern Solar Energy Research (ANSER) Center, Northwestern University, Evanston, Illinois 60208-3113, United States

[§]School of Engineering and Science, Jacobs University Bremen, Campus Ring 1, 28759 Bremen, Germany

Supporting Information

ABSTRACT: Artificial photosynthetic systems for solar energy conversion exploit both covalent and supramolecular chemistry to produce favorable arrangements of light-harvesting and redox-active chromophores in space. An understanding of the interplay between key processes for photosynthesis, namely light-harvesting, energy transfer, and photoinduced charge separation and the design of novel, self-assembling components capable of these processes are imperative for the realization of multifunctional integrated systems. We report our investigations on the potential of extended tetracationic cyclophane/perylene diimide systems as components for artificial photosynthetic applications. We show how the selection of appropriate heterocycles, as extending units, allows for tuning of the electron accumulation and photophysical properties of the extended tetracationic cyclophanes. Spectroscopic techniques confirm energy transfer between the extended tetracationic cyclophanes and perylene diimide is ultrafast and quantitative, while the heterocycle specifically influences the energy transfer related parameters and the acceptor excited state.



INTRODUCTION

The recently synthesized, extended tetracationic cyclophane,¹ **ExBox**⁴⁺, comprising two phenylene-extended bipyridinium units linked together by two *p*-xylylene (*p*-Xy) bridges to form a rectangular macrocycle, has received attention on account of its potential for inclusion in artificial photosynthetic systems. Numerous properties render **ExBox**⁴⁺ an attractive candidate for such applications, including ultrafast, intermolecular charge transfer from a suitable electron-rich guest,² intramolecular through-bond charge transfer from the *p*-Xy bridges to the extended bipyridinium units³ (**ExBIPY**²⁺) and multielectron accumulation^{1,3} leading to an array of accessible mixed-valence states. Most recently, we reported⁴ the first incidence of energy transfer (EnT), an essential process of all biological photosynthetic systems,^{5–10} within the extended tetracationic cyclophane (**Ex¹Box**) family. The discovery of EnT within **Ex¹Box** systems opens up new possibilities for greater complexity and biomimetic function with regard to their inclusion in switchable, photoactive, mechanically interlocked systems^{11,12} and light-harvesting arrays for device applications.^{13–15}

Perylene diimides (PDIs) have received much attention for their high thermal, chemical, electrochemical and photophysical stability.¹³ Recent studies have found particular suitability of this highly versatile family of compounds in applications such as organic photocatalysis¹⁶ and solar water splitting,^{17,18} one of the most important photosynthetic processes due to its potential to provide a large scale, clean source of carbon-free energy.¹⁹

We develop our understanding of the viability of combined **Ex¹Box**/PDI systems to act as components in artificial photosynthetic systems, on account of their electron-accumulation and light-harvesting properties.

In order to comprehensively characterize the **Ex¹Box**/PDI systems, we synthesized three series of **ExBIPY**²⁺ species. First, the extended methyl viologens²⁰ (**MExVs**) where phenylene, thiophene and selenophene are used as the extending units to yield **MPV**²⁺, **MTV**²⁺ and **MSeV**²⁺, respectively (as shown in the [Supporting Information](#)). The **MExVs** serve as controls for the second series, the **Ex¹Boxes**, the corresponding members of

Received: October 8, 2015

Published: November 9, 2015

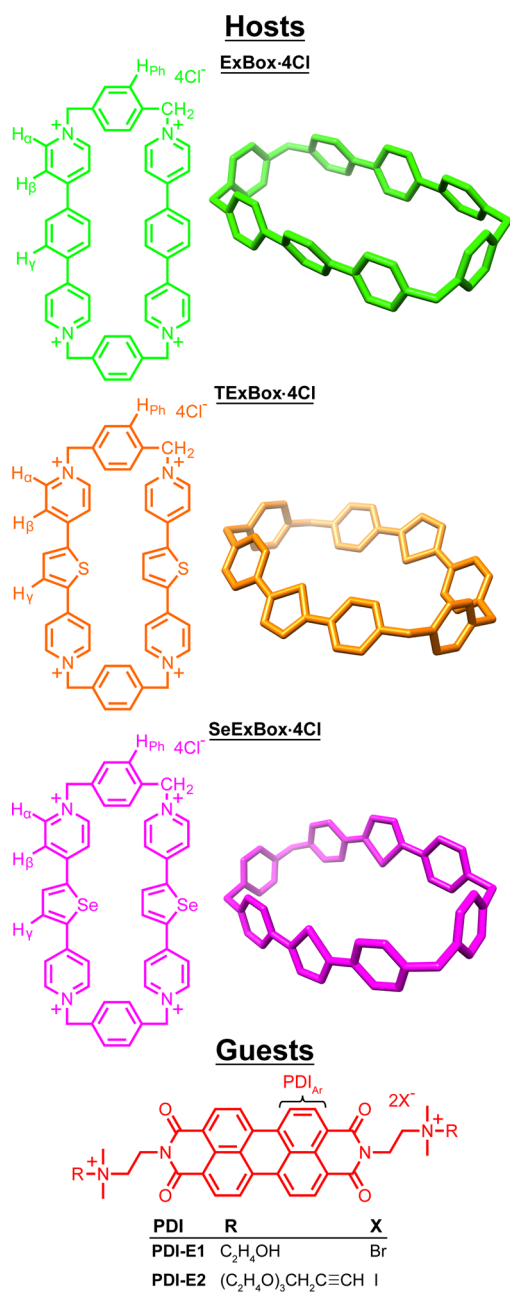


Figure 1. Structural formulas and X-ray crystal structures of ExBox-4Cl,¹ TExBox-4Cl, SeExBox-4Cl and the PDIs. PF₆⁻ counterions and solvent molecules have been removed for clarity.

which are ExBox⁴⁺, TExBox⁴⁺ and SeExBox⁴⁺ (Figure 1). The third series further increases the complexity of the ExBIPY²⁺ chemical environment via complexation and subsequent catenation^{21,22} of the Ex¹Boxes with a dicationic PDI derivative. The three Ex¹Box/PDI [2]catenanes (ExCats) are designated ExCat⁶⁺, TExCat⁶⁺ and SeExCat⁶⁺ (Figure 2).

RESULTS AND DISCUSSION

Synthesis and Structural Characterization. The MExVs, MTV²⁺ and MSeV²⁺, and Ex¹Boxes, TExBox⁴⁺ and SeExBox⁴⁺, were synthesized via analogous protocols¹ to MPV²⁺ and ExBox⁴⁺ (as detailed in the Supporting Information). TExBox⁴⁺ and SeExBox⁴⁺ were obtained in yields of 37% and 44%, respectively, which are significantly higher than the non-

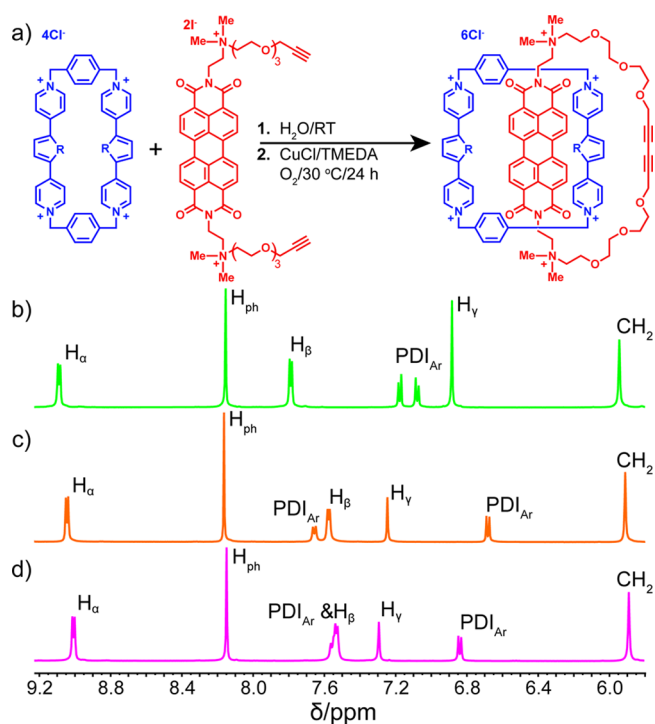


Figure 2. (a) Procedure for ExCat synthesis. R = C₂H₂ (ExBox⁴⁺/ExCat⁶⁺), S (TExBox⁴⁺/TExCat⁶⁺) and Se (SeExBox⁴⁺/SeExCat⁶⁺). ¹H NMR spectra (D₂O, 1 mM, Cl⁻ counterions) of (b) ExCat⁶⁺, (c) TExCat⁶⁺ and (d) SeExCat⁶⁺.

templated yield reported¹ for ExBox⁴⁺ (19%), presumably on account of the reduced symmetry of TExBox⁴⁺ and SeExBox⁴⁺, which induces lower bond angle strain in the transition state of the ring closing reaction. The ¹H NMR spectra of the Ex¹Boxes and their corresponding X-ray crystal structures are shown in Figures 1 and S1.

The Hay modification^{23,24} of the terminal alkyne Glaser homocoupling reaction^{23,24} in aqueous media was selected for the catenation procedure²⁵ (Figure 2) as complexation between the Ex¹Boxes and PDI-E1 was observed only in water and not in organic solvents (Figures S2–S4). Binding constants on the order of 10⁴ M⁻¹ were obtained by isothermal titration calorimetry (Figure S7). The reaction conditions employed consisted of an aerated aqueous solution of PDI-E2 (1 mM), three equivalents of Ex¹Box host and excesses of CuCl and tetramethylethylenediamine, stirred at 30 °C. Upon completion (monitored by analytical HPLC), the reaction mixture was centrifuged to remove the solid copper residue. The supernatant was subjected to reverse phase column chromatography and the fractions containing pure product, analyzed by analytical HPLC, were combined and lyophilized. The trifluoroacetate counterions were then exchanged for chloride counterions using tetrabutylammonium chloride (NBu₄Cl).

The catenanes, ExCat⁶⁺, TExCat⁶⁺ and SeExCat⁶⁺ were obtained in yields of 19%, 14% and 16%, respectively. ¹H NMR of the ExCats revealed shifts in the resonances associated with the Ex¹Box components nearly identical to those identified as complexed peaks via titrations (Figures 2, S2–S3, S5), while DOSY NMR revealed that both PDI and Ex¹Box components diffuse at equal rates (Figure S6). X-ray crystallography also confirmed the acquisition of the target compounds,²⁶ which reveal closely packed extended superstructures supported by an extensive network of CH–F interactions between the aromatic

hydrogen atoms of the Ex¹Boxes and fluorine atoms of the PF₆⁻ counterions (Figures S8–S9).

Electrochemical Characterization. Cyclic voltammetry (CV) of the MExVs, Ex¹Boxes and ExCats was performed in dimethyl sulfoxide (Me₂SO) at a concentration of 1 mM with a sweep rate of 50 mV s⁻¹ against a Ag/AgCl reference electrode. All redox couple potentials are summarized in Table 1. CV

Table 1. Electrochemical Half-Wave Redox Potentials of the MExVs, Ex¹Boxes and ExCats in Me₂SO

compound	1st $E_{1/2}$ (V) ^a	2nd $E_{1/2}$ (V) ^a	3rd $E_{1/2}$ (V) ^a
MPV ²⁺	-0.82	–	–
MTV ²⁺	-0.74	-0.85	–
MSeV ²⁺	-0.64	-0.76	–
ExBox ⁴⁺	-0.82	–	–
TExBox ⁴⁺	-0.49	-0.63	–
SeExBox ⁴⁺	-0.34	-0.46	–
ExCat ⁶⁺	-0.25	-0.48	-0.78
TExCat ⁶⁺	-0.21	-0.45	-0.68
SeExCat ⁶⁺	-0.21	-0.42	-0.61
PDI-E1	-0.34	-0.51	–

^aDetermined by cyclic voltammetry. A glassy carbon working electrode, an Ag/AgCl reference electrode and a platinum counter electrode were used to characterize 1 mM Me₂SO solutions of the hexfluorophosphate salts of the analytes at 298 K, with 0.1 M TBAPF₆ serving as the supporting electrolyte at a scan rate of 50 mVs⁻¹. Because of the closely overlapping peaks of SeExBox⁴⁺ and MSeV²⁺, an error of ±0.2 V is estimated for their half-wave redox potentials.

(Figure S10) reveals that each of the MExVs undergo two one-electron reductions. MPV²⁺ possesses the most negative reduction potential, which is smooth and nonbroadened, indicating little or no communication between the two pyridinium centers. MSeV²⁺ and MTV²⁺ possess more positive reduction potentials with small and significant shouldering, respectively, demonstrating progressively higher levels of communication.

Upon incorporation of the ExBIPY²⁺ units into the Ex¹Boxes, their redox properties are significantly altered (Figure S11). ExBox⁴⁺ reveals two overlapping two-electron reduction peaks without any obvious shouldering. The degree of communication within ExBox⁴⁺ in Me₂SO is significantly lower than that found in dimethylformamide¹ (DMF). TExBox⁴⁺ and SeExBox⁴⁺, in line with the previous trend, display more positive reduction potentials. There is also significantly greater separation of the two two-electron redox couples, indicating greater communication within TExBox⁴⁺ and SeExBox⁴⁺, which is attributed to higher conformational restriction of their constituent aromatic rings, on account of the lower symmetry of their extending units. A close examination of the X-ray crystal structures of the Ex¹Boxes supports the notion that their relative conformations in the solution phase and solid state are similar.

Cyclic voltammograms of the ExCats exhibit three distinct redox couples (Figure S12). The first two represent the first and second one-electron reductions of the PDI component. The ExCats also exhibit a third redox couple with a much higher peak current than the first two reduction events, which represents the four one-electron reductions of the Ex¹Box components. This is likely on account of structural distortion of the Ex¹Boxes by the PDI guest, which eliminates any communication between the pyridinium units, thus facilitating

their simultaneous reduction. As such, the Ex¹Box redox couples are smooth and nonbroadened. Thus, CV illustrates how all ExCats are capable of incrementally accepting up to six electrons, with tunable reduction potentials over a range of 570 mV (–210 to –780 mV), where the PDI component's reduction potential may be altered over 270 mV (–210 to –480 mV). The reversibility of the redox peaks illustrates good electrochemical stability at a 50 mV s⁻¹ scan rate.²⁷ The accessibility of various, stable mixed valence redox states is an essential property of artificial photosynthetic reaction centers, where the buildup of charge enables the realization of multielectron processes such as water splitting.^{28–30}

Steady-State Photophysical Characterization. Having investigated the structural and electrochemical properties of the three series, we moved onto their photophysical properties in water. Steady-state electronic absorption and fluorescence emission studies (Figure 3) show that MPV²⁺ and ExBox⁴⁺ possess the highest singlet excitation energy (¹*E_S) in their respective series, while MSeV²⁺ and SeExBox⁴⁺ possess the lowest. MTV²⁺ and TExBox⁴⁺ displayed the highest fluorescence quantum yields (Φ_f, 0.77 and 0.37, respectively), while MSeV²⁺ and SeExBox⁴⁺ displayed the lowest (0.0017 and

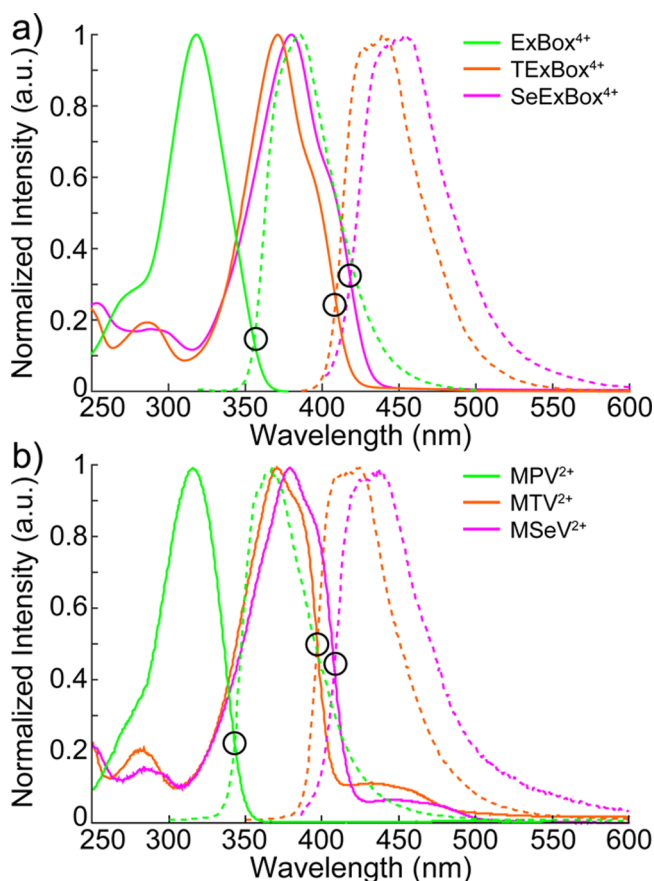


Figure 3. (a) Normalized electronic absorption (solid line) and fluorescence emission (dashed lines) spectra of ExBox⁴⁺ ($\lambda_{\text{ex}} = 319$ nm), TExBox⁴⁺ ($\lambda_{\text{ex}} = 371$ nm) and SeExBox⁴⁺ ($\lambda_{\text{ex}} = 380$ nm). (b) Normalized electronic absorption (solid line) and fluorescence emission (dashed lines) spectra of MPV²⁺ ($\lambda_{\text{ex}} = 315$ nm), MTV²⁺ ($\lambda_{\text{ex}} = 378$ nm) and MSeV²⁺ ($\lambda_{\text{ex}} = 378$ nm). All measurements were performed in water with Cl⁻ counterions. Black circles indicate the cross over points of absorption and emission spectra, which represent excited state singlet energies.

Table 2. Steady-State Photophysical Properties of the Ex¹Boxes and MExVs

compound	electronic absorption maximum (nm)	fluorescence emission maximum (nm) ^a	fluorescence quantum yield (Φ_f) ^b	singlet energy (eV) ^c	triplet energy (eV) ^d
ExBox ⁴⁺	318	386	0.21	3.48	2.14
MPV ²⁺	314	371	0.68	3.59	–
TExBox ⁴⁺	371	439	0.37	3.03	2.02
MTV ²⁺	370	416	0.77	3.11	–
SeExBox ⁴⁺	378	454	0.0027	2.96	1.94
MSeV ²⁺	380	434	0.0017	3.02	–

^aExcitation wavelengths (λ_{ex}) used for each ExTC/MExV corresponded to its electronic absorption maximum as detailed in the first column. ^bSee Supporting Information for conditions used for fluorescence quantum yield determination. ^cDetermined by the intersection of the normalized electronic absorption and fluorescence emission spectra. ^dDetermined by the peak maxima of the phosphorescence emission spectra. Triplet energies were not obtained for MExVs.

0.0027, respectively). The electronic absorption maxima show negligible shifting between the respective members of the MExV and Ex¹Box series. However, the fluorescence emission maxima of the Ex¹Boxes are all red-shifted relative to the MExVs. As such, the ¹*E_S of the Ex¹Boxes are approximately 0.08 eV lower than their respective MExVs. The above parameters are detailed in Table 2.

The steady-state electronic absorption and fluorescence emission spectra of the ExCats in water are shown in Figure 4. An essential property of any solar energy conversion device is the ability to absorb light within the solar spectrum as measured at the earth's surface.³¹ The spectral excitation window of ExBox⁴⁺ within ExCat⁶⁺, defined by the full width half-maximum of the electronic absorption profile, lies outside the visible spectrum. However, the lower HOMO–LUMO gap of TExBox⁴⁺ and SeExBox⁴⁺ within their corresponding ExCats, induced by the more electron rich 5-membered heterocycles, leads to an overlap of their excitation windows with the visible part of the solar spectrum. Thus, the light-harvesting properties of the Ex¹Boxes may be tuned by changing the identity of the extending unit and in conjunction with the PDI component, the ExCats are able to absorb over most of the solar spectrum. The excitation windows of the Ex¹Boxes within the ExCats are detailed in Table 4.

Lastly, the fluorescence excitation spectra of the ExCats (Figure 4, $\lambda_{mon} = 550$ nm) bear very strong similarity to their corresponding absorption spectra within the absorption region of the Ex¹Box components, clearly illustrating the EnT process active between the ExBIPY²⁺ and PDI chromophores.

Time-Resolved Photophysical Characterization. Time-resolved photophysical experiments were next carried out in water to gain a greater insight into the excited state dynamics of the Ex¹Boxes and EnT dynamics of the ExCats. All excited state relaxation time constants are detailed in Table 3.

First, the MExVs were investigated by femtosecond transient absorption (fsTA). We do not observe ground state bleaching of the MExVs or Ex¹Boxes due to a combination of the strong, overlapping absorption of the transient species with the ground state absorption and the 430 nm edge of the probe window. MPV²⁺, MTV²⁺ and MSeV²⁺ were excited at 330, 414, and 414 nm, respectively, with 150 fs pulses. Upon excitation of MPV²⁺, the first excited singlet state, ¹*MPV²⁺, is produced, which decays with an effective lifetime, $\tau_{eff} = 1330 \pm 15$ ps, by fluorescence to the ground state, ⁰MPV²⁺ (Figures S13–S14). Time-correlated single photon counting (TCSPC) recorded a similar lifetime of $\tau_{eff} = 1.40$ ns (Figure S35). Spin–orbit intersystem crossing (SO-ISC) affords a minor contribution to the decay, producing the first excited triplet state, ³*MPV²⁺,

whose decay persists beyond 7 ns, the experimental time scale of our fsTA setup. Indeed, all triplet states investigated below occurred beyond this time scale.

¹*MTV²⁺ decayed in $\tau_{eff} = 1080 \pm 8$ ps by fsTA (Figures S13, S15), while TCSPC recorded a slightly longer lifetime of $\tau_{eff} = 1.85$ ns (Figure S35). SO-ISC again affords a small contribution decay, yielding ³*MTV²⁺. MSeV²⁺ displayed markedly different behavior (Figures S13, S16). ¹*MSeV²⁺ decayed rapidly via SO-ISC to produce ³*MSeV²⁺ in $\tau_{eff} = 5.1 \pm 0.1$ ps. The almost exclusive contribution of SO-ISC to the decay kinetics³² is attributed to the internal heavy atom effect³³ facilitated by the selenium atom, which also manifests in the Φ_f of MSeV²⁺ (see Table 2).

The Ex¹Boxes were then investigated under the same conditions used for the MExVs (Figures 5, S17). A schematic illustration of the excited state dynamics of all Ex¹Boxes in water is shown in Scheme 1.

The initial fsTA spectrum of TExBox⁴⁺ is characterized by absorptions at 482, 734, 1081, and 1246 nm, which are assigned to ¹*TExBox⁴⁺ (Figure S19), which decays via two parallel pathways in $\tau_{eff} = 447 \pm 4$ ps. The first pathway is via fluorescence to ⁰TExBox⁴⁺ (Figure 3), the lifetime of which (τ_f) may be estimated by the effective lifetime of ¹*MTV²⁺. The second pathway is the intramolecular, through-bond reduction of ExBIPY²⁺ by the *p*-Xy bridge, resulting in a photoinduced charge separated state,³ TExBIPY⁺-*p*-Xy⁺, in a time, τ_{PCS} , characterized by absorbances at 576, 918, and 1065 nm.

$$\frac{1}{\tau_{eff}} = \frac{1}{\tau_f} + \frac{1}{\tau_{PCS}} \quad (1)$$

The relation between τ_{eff} , τ_f and τ_{PCS} is given by eq 1. Thus, the approximation, $\tau_{PCS} \approx 763$ ps, may be calculated. Visible-infrared spectroelectrochemistry corroborated the TExBIPY⁺-*p*-Xy⁺ assignment. The spectrum reveals maxima at 578, 924, and 1066 nm (Figure S37), which is nearly identical to the reconstituted fsTA spectrum. The approximate free energy of photoinduced charge separation (PCS), ΔG_{PCS} , defined as the difference between the Ex¹Box singlet energy (see Table 2), and the ion pair energy of the photoinduced charge separated state, ΔG_{IP} (see eq 2) was then calculated.

$$\Delta G_{PCS} = \Delta G_{IP} - {}^1E \quad (2)$$

$$\Delta G_{IP} = E_{ox} - E_{red} + \Delta U + \Delta G_{solv} \quad (3)$$

ΔG_{IP} may be calculated by the equation developed by Weller³⁴ (eq 3). E_{ox} is the oxidation potential of the *p*-Xy bridge (1.98 V vs Ag/AgCl),³⁵ and E_{red} is the first reduction potential of the ExBIPY²⁺ unit, here taken as the first reduction potential

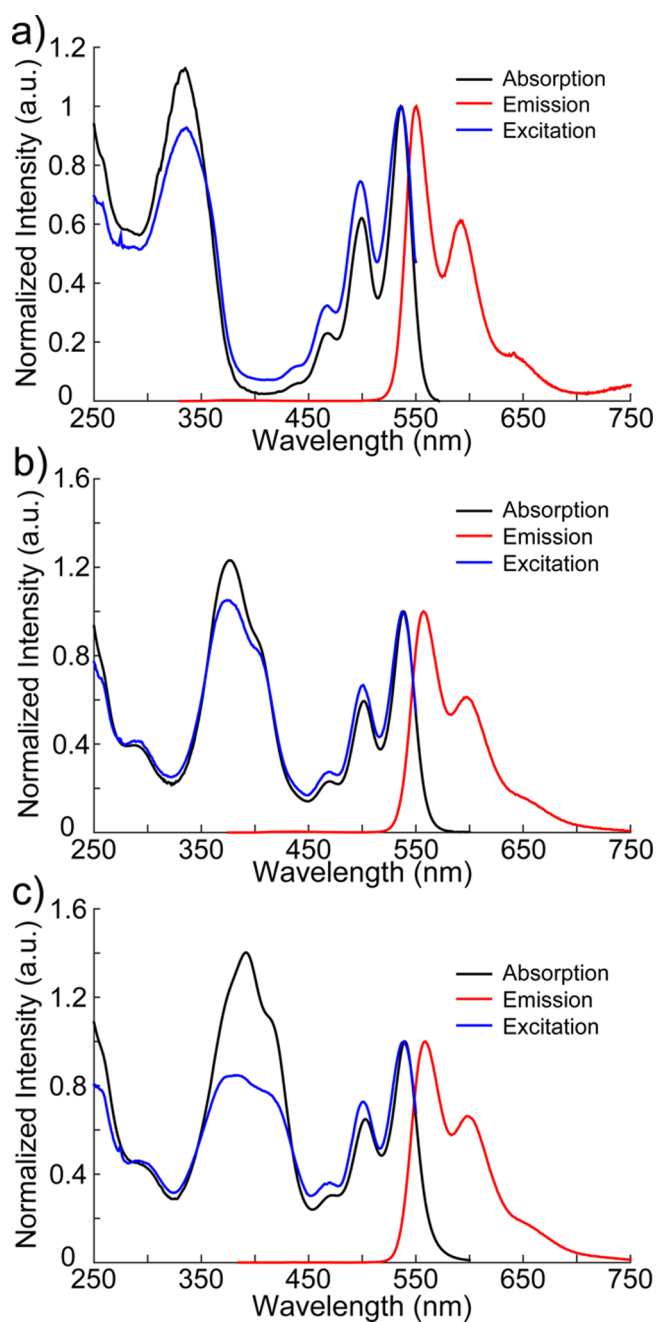


Figure 4. Normalized absorption, excitation ($\lambda_{\text{mon}} = 550$ nm) and emission spectra of (a) ExCat^{6+} ($\lambda_{\text{ex}} = 320$ nm), (b) TExCat^{6+} ($\lambda_{\text{ex}} = 377$ nm), and (c) SeExCat^{6+} ($\lambda_{\text{ex}} = 392$ nm). All measurements were performed in water with Cl^- counterions.

of the corresponding MExV (see Table 1). ΔU , a Coulombic correction factor, may be neglected as it has been shown to be small in ExBox^{4+} in polar media.³ ΔG_{solvr} , a solvent correction factor, may also be neglected on account of the high dielectric constants of water and Me_2SO . Thus, in the case of TExBox^{4+} , ΔG_{PCS} is found to be approximately -0.31 eV, illustrating that PCS is an energetically downhill and spontaneous process.

Charge recombination then occurs in $\tau_{\text{CR}} = 2850 \pm 60$ ps, resulting in the formation of ${}^3\text{TExBox}^{4+}$, via spin-orbit charge transfer intersystem crossing³⁶ (SOCT-ISC), on account of the favorable perpendicular orientation of the ExBIPY^{2+} and $p\text{-Xy}$ chromophores, characterized by absorbances at 576, 914, and 1062 nm. The quantum yield for the formation of ${}^3\text{TExBox}^{4+}$

Table 3. Time Constants (τ , ps) for the Decay of the Singlet Excited States of the MExVs and Ex¹Boxes, as Measured by Femtosecond Transient Absorption Spectroscopy in Water

compound	${}^1\text{singlet}(h)^a$	${}^1\text{singlet}$	decay mechanism ^b
ExBox^{4+}	73 ± 10	413 ± 7	see text
MPV^{2+}	96 ± 1	1330 ± 15	Fluorescence, IC
TExBox^{4+}	–	447 ± 4	Fluorescence, PCS ^c
MTV^{2+}	71 ± 2	1080 ± 8	Fluorescence, IC
SeExBox^{4+}	–	6.6 ± 0.1	SO-ISC
MSeV^{2+}	–	5.1 ± 0.1	SO-ISC

^a(h) indicates a vibrationally excited state. ^bIC = internal conversion, SO-ISC = spin-orbit intersystem crossing. ^cPCS = photoinduced charge separation. Charge recombination occurs with a lifetime of 2850 ps.

in solution is unknown, as charge recombination to ${}^0\text{TExBox}^{4+}$ likely occurs in parallel with SOCT-ISC.

${}^3\text{TExBox}^{4+}$ was then investigated in the solid state via phosphorescence emission spectroscopy (PES, Me_2SO , 77 K, Figure S38), which displayed an emission signal with a maximum at 614 nm, giving a triplet energy (1E_T) of 2.02 eV. Time-resolved phosphorescence emission spectroscopy (TRPES, Me_2SO , 77 K, $\lambda_{\text{mon}} = 614$ nm) revealed a solid state lifetime of $\tau_p = 10.6$ ms, which is typical for organic compounds under such conditions.³¹

The fsTA spectrum³⁷ of ${}^1\text{SeExBox}^{4+}$ is characterized by four absorbances at 497, 758, 1160, and 1309 nm. ${}^1\text{SeExBox}^{4+}$ is very short-lived, decaying in $\tau_{\text{eff}} = 6.6 \pm 0.1$ ps, principally via SO-ISC to ${}^3\text{SeExBox}^{4+}$, characterized by absorbances at 475, 890, and 1027 nm. This singlet lifetime is very similar to that of ${}^1\text{MSeV}^{2+}$, while the Φ_f of SeExBox^{4+} (see Table 2) demonstrates that fluorescence contributes negligibly to singlet decay. Relaxation of ${}^3\text{SeExBox}^{4+}$ occurs in $\tau_{\text{eff}} = 2280 \pm 870$ ps. On the basis of the spectral similarities of the 2 ns component (Figures 5, S20) to ${}^3\text{SeExBox}^{4+}$, it is attributed to triplet-triplet annihilation arising from collisional deactivation of ${}^3\text{SeExBox}^{4+}$ with either another ${}^3\text{SeExBox}^{4+}$ species or triplet oxygen (solutions were not deoxygenated prior to the laser experiments). Residual ${}^3\text{SeExBox}^{4+}$ persists beyond 7 ns. The high efficiency of SO-ISC means that it kinetically outcompetes PCS. As such, despite the negative ΔG_{PCS} for SeExBox^{4+} (approximately -0.35 eV), no evidence for $\text{SeExBIPY}^+p\text{-Xy}^+$ (Figure S37) was observed in the fsTA spectra. ${}^3\text{SeExBox}^{4+}$ was further probed using nanosecond transient absorption (nsTA, Figures S31–S32), which revealed a short triplet lifetime of $\tau_{\text{eff}} = 2.80 \pm 0.01$ μs in oxygenated solution at room temperature.

PES (Me_2SO , 77 K) revealed a signal with a peak maximum at 640 nm, yielding a 1E_T of 1.94 eV (Figure S38). TRPES ($\lambda_{\text{mon}} = 640$ nm) revealed a triplet lifetime of $\tau_p = 0.2$ ms, which is 2 orders of magnitude greater than that measured using nsTA. Although fairly typical for organic phosphorescent compounds, this lifetime is still relatively short given the efficiency of triplet formation, which is likely on account of the internal heavy atom effect, which increases the rate of SO-ISC from ${}^3\text{SeExBox}^{4+}$ to ${}^0\text{SeExBox}^{4+}$.

Although already documented in organic media,³ we repeated our studies of the excited state dynamics of ExBox^{4+} in water. Upon excitation, ${}^1\text{ExBox}^{4+}$ is produced, characterized by a single, intense absorbance at 499 nm, very similar to that observed in MeCN ,³ and a rising absorbance into the NIR region, which undergoes initial relaxation in $\tau_r = 73 \pm 1$ ps.

Table 4. Photophysical Properties of the ExCats in Water

compound	Förster distance (Å) ^a	fluorescence quantum yield ^b	fluorescence lifetime (τ , ns) ^c	excitation window (nm) ^d	PDI ¹ *singlet lifetime (τ , ns) ^e
ExCat ⁶⁺	26.3 ^f	0.90	6.30	293–360 (335)	5.85 \pm 0.03
TExCat ⁶⁺	37.9	0.76	6.45	351–414 (377)	6.63 \pm 0.03
SeExCat ⁶⁺	18.2	0.18	1.75	355–430 (391)	1.56 \pm 0.04

^aDetermined using the absorption spectrum of PDI-E1 C CB[8] as an approximation for the disaggregated absorption spectrum of PDI in water and a κ^2 value of 2/3. ^bDetermined by relative measurement with Rhodamine 6G in ethanol as fluorescence quantum yield standard ($\Phi_f = 0.95$). ^cDetermined by TCSPC. Excitation wavelength (λ_{ex}) = 510 nm, monitored wavelength (λ_{mon}) = 550 nm, error $\pm 3\%$. ^dDefined as the fwhm of the ExTC^{1*} \leftarrow ⁰S absorption peaks (absorption maxima are shown in parentheses). ^eDetermined by fsTA. Indirect excitation (λ_{ex} = 330 nm for ExCat⁶⁺; λ_{ex} = 414 nm for TExCat⁶⁺ and SeExCat⁶⁺). ^fFrom ref 4.

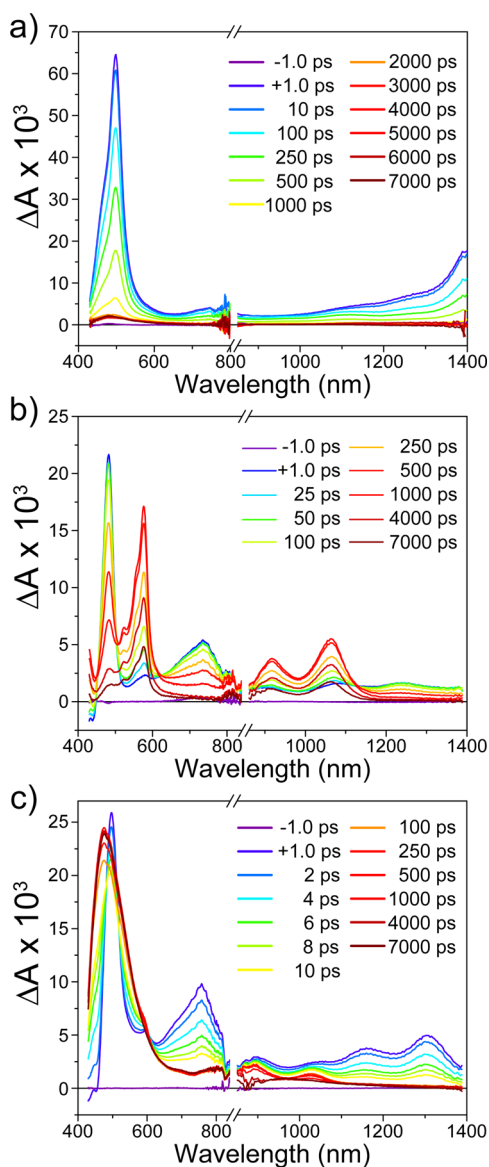


Figure 5. Combined visible and near-infrared femtosecond transient absorption spectra of (a) ExBox⁴⁺ (λ_{ex} = 330 nm, 0.4 $\mu\text{J pulse}^{-1}$), (b) TExBox⁴⁺ (λ_{ex} = 414 nm, 1.0 $\mu\text{J pulse}^{-1}$) and (c) SeExBox⁴⁺ (λ_{ex} = 414 nm, 1.0 $\mu\text{J pulse}^{-1}$). Relative amplitudes on either side of the vertical break are arbitrary. All measurements were performed in water with Cl⁻ counterions.

¹*ExBox⁴⁺ decays further in $\tau_{\text{eff}} = 413 \pm 10$ ps, and is replaced by a ³*ExBox⁴⁺, characterized by a single peak at 490 nm. Interestingly, evolution of ExBIPY⁺-*p*-Xy⁺, previously observed

upon decay of ¹*ExBox⁴⁺ in MeCN and characterized by a broad 900–1200 nm absorbance, is not observed in water.

The absence of an observed ExBIPY⁺-*p*-Xy⁺ state was an unexpected result given the strong driving force for PCS.³ As the decay of ¹*ExBox⁴⁺ is approximately three times shorter than that of ¹*MPV²⁺, it is unlikely that ¹*ExBox⁴⁺ decays directly to ⁰ExBox⁴⁺ and ³*ExBox⁴⁺. Inverted reaction kinetics, whereby the formation of the ExBIPY⁺-*p*-Xy⁺ state is much slower than its decay via charge recombination, is the most likely explanation. A simplified analysis of the kinetics of charge recombination, using Marcus–Hush theory (see Supporting Information), shows that the rate is approximately 13 times faster in water than in MeCN. Using eq 1 and the lifetime of ¹*MPV²⁺ as an approximation for τ_{β} one may postulate $\tau_{\text{PCS}} \approx 599$ ps for ¹*ExBox⁴⁺, which is similar to that calculated for ¹*TExBox⁴⁺.

PES (Me₂SO, 77 K) revealed an ExBox⁴⁺ triplet energy of 2.14 eV, while TRPES (λ_{mon} = 515 nm) was best fitted using a biexponential function with time constants $\tau_{p1} = 0.29$ s (26%) and $\tau_{p2} = 0.94$ s (74%). The approximate one second phosphorescence lifetime of ³*ExBox⁴⁺ is on the long end of the scale for organic molecules.^{38–40}

Having characterized the relaxation dynamics of the Ex¹Boxes, we turned our attention to the energy transfer dynamics of the ExCats. Investigations by fsTA were conducted using pump pulse wavelengths that selectively excite the Ex¹Box donors (Figures 6, S21). Schematic descriptions of the ExCat relaxation dynamics are shown in Scheme 2.

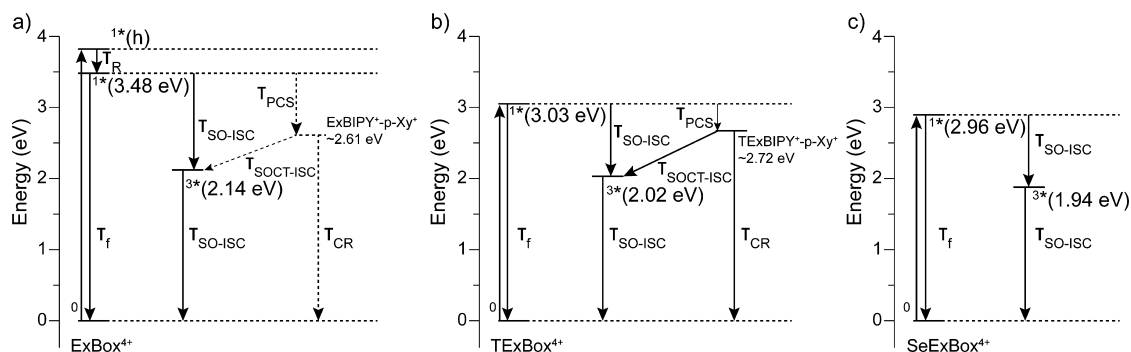
In all cases, the first excited singlet states of the Ex¹Box donors were not observed at all upon photoexcitation (Figures S22–S24), indicating excited state deactivation occurs within the 250 fs response time of the instrument. We can, therefore, conclude that the excited singlet states of the Ex¹Boxes within the three ExCats have lifetimes of less than 250 fs.

$$\eta = \frac{1}{1 + \tau'/\tau} \quad (4)$$

Eq 4 (τ = deactivation lifetime of the donor by all pathways in the absence of the acceptor (measured by fsTA above, see Table 3), τ' = lifetime of the energy transfer process between donor and acceptor) may then be used to calculate the EnT efficiency (η) between PDI and the three Ex¹Boxes. Taking τ' to be less than 250 fs, η is found to be greater than 99.99% for ExCat⁶⁺ and TExCat⁶⁺, demonstrating that EnT is quantitative. In the case of SeExCat⁶⁺, η is found to be greater than 96%, which is particularly remarkable, given its essentially zero fluorescence quantum yield ($\Phi_f < 0.002$).

Such high EnT efficiencies are facilitated by the small donor–acceptor separations within the catenane structure (~ 3.5 Å). The crystal structures of the catenanes show that the van der Waals radii of the PDI and Ex¹Box components

Scheme 1. Energetics and Excited State Relaxation Dynamics for Fluorescence (τ_f), Spin-Orbit Intersystem Crossing ($\tau_{\text{SO-ISC}}$), Photoinduced Charge Separation (τ_{PCS}), Spin-Orbit Charge Transfer Intersystem Crossing ($\tau_{\text{SOCT-ISC}}$) and Charge Recombination (τ_{CR}) in (a) ExBox⁴⁺, (b) TExBox⁴⁺ and (c) SeExBox⁴⁺^a



^aDashed lines indicate hypothesized processes. All time constants are described in the text and Table 3.

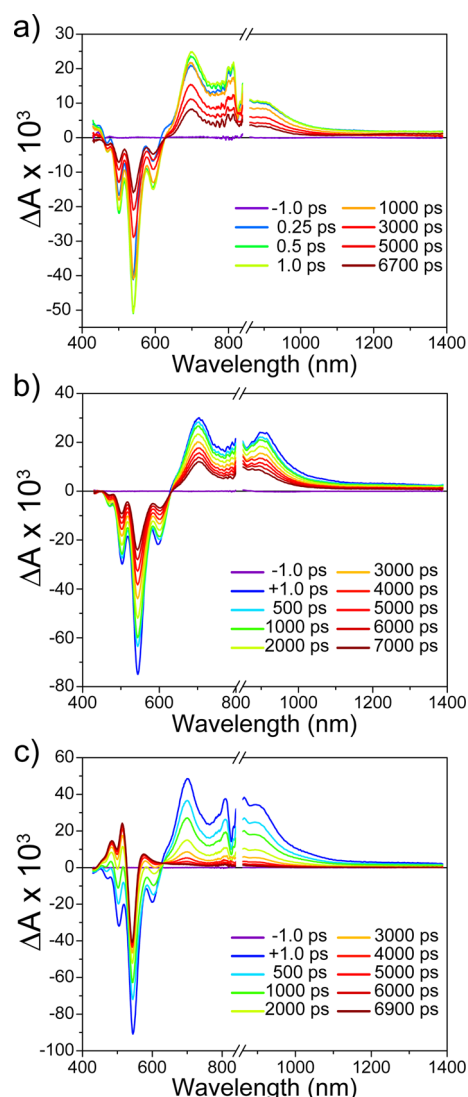


Figure 6. Combined visible and near-infrared femtosecond transient absorption spectra of (a) ExCat⁶⁺ ($\lambda_{\text{ex}} = 330 \text{ nm}$, $0.4 \mu\text{J pulse}^{-1}$), (b) TExCat⁶⁺ ($\lambda_{\text{ex}} = 414 \text{ nm}$, $1.0 \mu\text{J pulse}^{-1}$) and (c) SeExCat⁶⁺ ($\lambda_{\text{ex}} = 414 \text{ nm}$, $1.0 \mu\text{J pulse}^{-1}$). Relative amplitudes on either side of the vertical break are arbitrary. All measurements were performed in water with Cl⁻ counterions.

overlap, such that molecular orbital overlap should allow EnT to proceed via the electron exchange Dexter mechanism,⁴¹ which is likely the dominant mechanism. The documentation of ultrafast charge transfer (<250 fs) between ExBox⁴⁺ and perylene² demonstrates that such a mechanism involving electron exchange is certainly feasible. Although Förster theory⁴² predicts critical transfer radii (see Table 4) such that EnT should be quantitative within the catenanes, at a donor–acceptor separation of 3.5 Å the point dipole approximation of Förster theory breaks down. However, a short-range multipolar description of EnT could, potentially, also account for the observed rate. Such an approach has been previously used to describe EnT within natural photosynthetic systems.⁴³

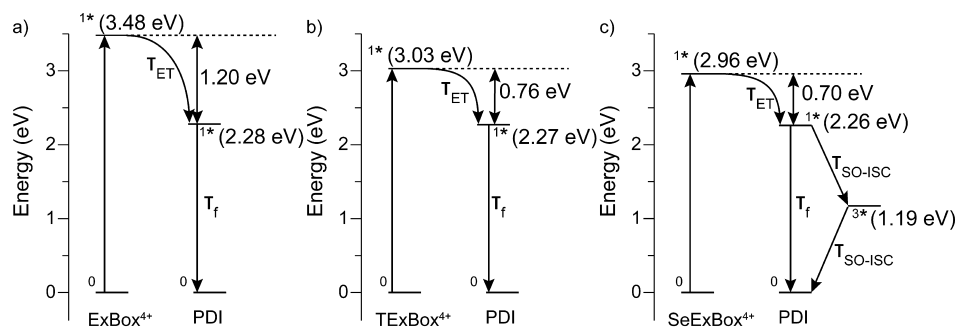
Subsequent relaxation of the excited PDI components was further monitored. fsTA reveals that ¹*PDI is fully evolved within 1 ps for all ExCats (Figures 6, S22–S24). In both ExCat⁶⁺ and TExCat⁶⁺, the ground state bleach (445–580 nm), stimulated emission (575–630 nm), and excited state absorption features, in both visible and NIR regions, all decay with the same time constants as determined by a global fit to all of these features (see Figure S22–S23), which is in good agreement with the fluorescence lifetimes determined by TCSPS. ¹*PDI decays to the ground state mainly via fluorescence with a time constant of $\tau_{\text{eff}} = 5.85 \pm 0.03 \text{ ns}$, for ExCat⁶⁺ and $\tau_{\text{eff}} = 6.63 \pm 0.03 \text{ ns}$ for TExCat⁶⁺.

SeExCat⁶⁺, once again, displayed very different behavior. Upon excitation, we immediately observe the ¹*PDI spectrum. The stimulated emission and excited state absorption bands decay very quickly (fsTA, $\tau_{\text{eff}} = 1.56 \pm 0.04 \text{ ns}$), while the PDI ground state bleach at approximately 530 nm remains throughout the experimental window. The higher energy PDI bleaches also remain, but rise with a similar time constant (global fitting, Figure S24) from the formation of a positive overlapping absorption corresponding to ³*PDI, characterized⁴⁴ by peak maxima at 485, 514, and 576 nm.

$$\frac{1}{\tau_{\text{eff}}} = \frac{1}{\tau_f} + \frac{1}{\tau_{\text{ISC}}} \quad (5)$$

Assuming $\tau_f = 3.7 \text{ ns}$ for ¹*PDI (taken from the fsTA analysis of the inclusion complex,⁴⁵ PDI-E1CCB[8], Figures S29–S30), τ_{ISC} may be calculated using eq 5, yielding $\tau_{\text{ISC}} \approx 2.7 \text{ ns}$. TCSPC recorded a ¹*PDI lifetime of $\tau_{\text{eff}} = 1.75 \text{ ns}$ (Figure S36), which is in good agreement with fsTA, while Φ_f is heavily quenched (0.18) relative to ExCat⁶⁺ and TExCat⁶⁺ (0.90 and 0.77, respectively). The value of $\tau_f = 3.7 \text{ ns}$ for PDI-E1CCB[8]

Scheme 2. Energetics and Dynamics for Photodriven Energy Transfer (τ_{ET}), Fluorescence (τ_f) and Spin-Orbit Intersystem Crossing ($\tau_{\text{SO-ISC}}$) in (a) ExCat⁶⁺, (b) TExCat⁶⁺, and (c) SeExCat^{6+a}



^{a1*}T PDI energy from ref 46. All time constants are described in the text and Table 4.

is similar to that of destacked PDIs measured in organic media,⁴⁶ indicating that the polarity of the CB[8] cavity is similar to that of organic solvents. However, as the cavities of the Ex¹Boxes are smaller than that of CB[8], the micro-environments of their respective cavities are likely to be different. Therefore, one may also approximate the fluorescence lifetime of SeExCat⁶⁺ as $\tau_f \approx 6$ ns (similar to that of ExCat⁶⁺), which yields a value of $\tau_{\text{ISC}} \approx 2.1$ ns. Comparison of the ^{1*}PDI relaxation dynamics upon direct excitation ($\lambda_{\text{ex}} = 540$ nm) reveals similar behavior to that observed upon indirect excitation (Figures S25–S28).

SeExCat⁶⁺ was further investigated by nsTA and transient continuous wave electron paramagnetic resonance (TCW-EPR) to probe ^{3*}PDI. nsTA revealed a short triplet lifetime of $\tau_{\text{eff}} = 5.28 \pm 0.03$ μs in oxygenated solution at room temperature (Figures S33–S34), while TCW-EPR (85 K, Figure S39) shows the characteristic emission(e)–absorption-(a) polarization pattern, e,e,e,a,a,a, for ^{3*}PDI formed via SO-ISC.⁴⁷ As such, SeExCat⁶⁺ represents noncovalent method to generate the triplet state of a large, monomeric, aromatic chromophore in high yield in aqueous media via the external heavy atom effect, where El Sayed's selection rules formally forbid ^{1*}T(π – π^*) \leftarrow ^{1*}S(π – π^*) SO-ISC.

CONCLUSION

Our work illustrates how extending components may be used to tune the light-harvesting antenna properties of Ex¹Boxes to cover a significant portion of the solar spectrum and generate a high energy, singlet state PDI in quantitative yield via energy transfer. As such, the alteration of the chemical environment of extended bipyridiniums allows for the tailored design of a family of organic, optoelectronic materials, exhibiting excellent electron accumulation properties, capable of incrementally accepting and stabilizing up to six electrons with tunable redox potentials. Such properties afford potential for these materials in light-harvesting and catalytic applications, ranging from multielectron catalytic processes, such as water splitting, to organic synthetic photocatalysis in water. Our work has also expanded our understanding of the excited state behavior of Ex¹Boxes, illustrating their phosphorescence properties.

A drawback is that upon tuning the HOMO–LUMO gap of ExBIPY²⁺s using heavy atoms, energy is lost in the excited state PDI upon conversion to the triplet state. This could be circumvented by using fused heterocycle extending components as an alternative means to achieving solar spectrum coverage outside the presented range. Nevertheless, the ability

of SeExCat⁶⁺ to efficiently access PDI triplet states in high triplet quantum yields could find utility in triplet photosensitizing applications⁴⁸ in both aqueous and organic media. SeExCat⁶⁺ also demonstrates how the design element of the ExCats allows for highly efficient EnT from an essentially nonfluorescent antenna.

The mono and higher-order functionalization of Ex¹Boxes⁴⁹ and PDIs¹³ may also allow for the synthesis of novel ExCat derivatives capable of incorporating extra chromophores for additional electronic function and of surface attachment via multiple chemistries.

ASSOCIATED CONTENT

Supporting Information

The Supporting Information is available free of charge on the ACS Publications website at DOI: 10.1021/jacs.5b10329.

Details of synthetic procedures and characterization (NMR, HRMS) data for all new compounds, crystallographic characterization for TExBox-4PF₆, SeExBox-4PF₆, ExCat-6PF₆ and SeExCat-6PF₆, additional fsTA, nsTA, TCW-EPR, TCSPC, CV, ITC, electronic absorption, fluorescence and phosphorescence characterization data. (PDF)

ExCat-6PF₆ crystal structure. (CIF)

SeExCat-6PF₆ crystal structure. (CIF)

TExBox-4PF₆ and SeExBox-4PF₆ crystal structure. (CIF)

AUTHOR INFORMATION

Corresponding Author

*oas23@cam.ac.uk

Notes

The authors declare no competing financial interest.

ACKNOWLEDGMENTS

S.T.J.R. thanks the Cambridge Home and European Scholarship Scheme and the Robert Gardiner memorial scholarship. S.T.J.R., A.F. and O.A.S. thank the ERC starting investigator grant ASPiRe (project no. 240629) and the EPSRC (reference no. EP/G060649/1). Femtosecond and nanosecond spectroscopy (R.M.Y.), EPR spectroscopy (M.D.K.) and phosphorescence spectroscopy (Y.W.) were supported as part of the ANSER Center, an Energy Frontier Research Center funded by the U.S. Department of Energy, Office of Science, Office of Basic Energy Sciences under award no. DE-SC0001059. J.F.S.,

J.J.H., N.H., N.A.V. and E.D.J. acknowledge the Joint Center of Excellence in Integrated Nano-Systems (JCIN) between KACST and Northwestern University (Project 34-946) for their continued financial support. E.J.D. acknowledges NSF and Ryan fellowships. A.H. and W.M.N. thank the COST Action CM1005 "Supramolecular Chemistry in Water" and the DFG (grant NA-686/5) for financial support. The authors also thank Charlotte L. Stern and Dr. Amy A. Sarjeant for helpful discussions and Mr. Michael J. Byrne for his artistic contribution.

REFERENCES

- (1) Barnes, J. C.; Juríček, M.; Strutt, N. L.; Frascioni, M.; Sampath, S.; Giesener, M. A.; McGrier, P. L.; Bruns, C. J.; Stern, C. L.; Sarjeant, A. A.; Stoddart, J. F. *J. Am. Chem. Soc.* **2013**, *135*, 183–192.
- (2) Young, R. M.; Dyar, S. M.; Barnes, J. C.; Juríček, M.; Stoddart, J. F.; Co, D. T.; Wasielewski, M. R. *J. Phys. Chem. A* **2013**, *117*, 12438–12448.
- (3) Dyar, S. M.; Barnes, J. C.; Juríček, M.; Stoddart, J. F.; Co, D. T.; Young, R. M.; Wasielewski, M. R. *Angew. Chem., Int. Ed.* **2014**, *53*, 5371–5375.
- (4) Ryan, S. T. J.; Del Barrio, J.; Ghosh, I.; Biedermann, F.; Lazar, A. I.; Lan, Y.; Coulston, R. J.; Nau, W. M.; Scherman, O. A. *J. Am. Chem. Soc.* **2014**, *136*, 9053–9060.
- (5) Pullerits, T.; Sundström, V. *Acc. Chem. Res.* **1996**, *29*, 381–389.
- (6) McDermott, G.; Prince, S. M.; Freer, A. A.; Hawthornthwaite-Lawless, A. M.; Papiz, M.; Cogdell, R. J.; Isaacs, N. *Nature* **1995**, *374*, 517–521.
- (7) Kühlbrandt, W.; Wang, D. N. *Nature* **1991**, *350*, 130–134.
- (8) Kühlbrandt, W.; Wang, D. N.; Fujiyoshi, Y. *Nature* **1994**, *367*, 614–621.
- (9) Kühlbrandt, W. *Nature* **1995**, *374*, 497–498.
- (10) Barber, J., Ed.; *Primary Processes of Photosynthesis*; Elsevier Scientific Pub. Co.: Amsterdam, 1977.
- (11) Stoddart, J. F. *Angew. Chem., Int. Ed.* **2014**, *53*, 11102–11104.
- (12) Coskun, A.; Spruell, J. M.; Barin, G.; Dichtel, W. R.; Flood, A. H.; Botros, Y. Y.; Stoddart, J. F. *Chem. Soc. Rev.* **2012**, *41*, 4827–4859.
- (13) Huang, C.; Barlow, S.; Marder, S. R. *J. Org. Chem.* **2011**, *76*, 2386–2407.
- (14) Zhan, X.; Facchetti, A.; Barlow, S.; Marks, T. J.; Ratner, M. A.; Wasielewski, M. R.; Marder, S. R. *Adv. Mater.* **2011**, *23*, 268–284.
- (15) Li, C.; Liu, M.; Pschirer, N. G.; Baumgarten, M.; Müllen, K. *Chem. Rev.* **2010**, *110*, 6817–6855.
- (16) Ghosh, I.; Ghosh, T.; Bardagi, J. I.; König, B. *Science* **2014**, *346*, 725–728.
- (17) Ronconi, F.; Syrgiannis, Z.; Bonasera, A.; Prato, M.; Argazzi, R.; Caramori, S.; Cristino, V.; Bignozzi, C. A. *J. Am. Chem. Soc.* **2015**, *137*, 4630–4633.
- (18) Weingarten, A. S.; Kazantsev, R. V.; Palmer, L. C.; McClendon, M.; Koltonow, A. R.; Samuel, A. P. S.; Kiebal, D. J.; Wasielewski, M. R.; Stupp, S. I. *Nat. Chem.* **2014**, *6*, 964–970.
- (19) Quaschnig, V. *Renewable Energy and Climate Change*; John Wiley & Sons, Ltd: New York, 2010; pp 70–86.
- (20) Takahashi, K.; Nihira, T.; Akiyama, K.; Ikegami, Y.; Fukuyo, E. *J. Chem. Soc., Chem. Commun.* **1992**, 620–622.
- (21) Sauvage, J.-P.; Dietrich-Buchecker, C., Eds.; *Molecular Catenanes, Rotaxanes and Knots: A Journey through the World of Molecular Topology*; Wiley-VCH: Weinheim, 1999.
- (22) Wang, W.; Wang, L.; Palmer, B. J.; Exarhos, G. J.; Li, A. D. Q. *J. Am. Chem. Soc.* **2006**, *128*, 11150–11159.
- (23) Hay, A. S. *J. Org. Chem.* **1962**, *27*, 3320–3321.
- (24) Fomina, L.; Vazquez, B.; Tkatchouk, E.; Fomine, S. *Tetrahedron* **2002**, *58*, 6741–6747.
- (25) Fang, L.; Basu, S.; Sue, C.-H.; Fahrenbach, A. C.; Stoddart, J. F. *J. Am. Chem. Soc.* **2011**, *133*, 396–399.
- (26) Attempts to grow single crystals of TExCat⁶⁺ suitable for X-ray diffraction have, thus far, been unsuccessful.
- (27) Kaifer, A. E.; Gómez-Kaifer, M. *Supramolecular Electrochemistry [Electronic Resource]*; Wiley-VCH: Weinheim, 1999.
- (28) Arachchige, S. M.; Brown, J. R.; Chang, E.; Jain, A.; Zigler, D. F.; Rangan, K.; Brewer, K. J. *Inorg. Chem.* **2009**, *48*, 1989–2000.
- (29) Oliva, M. M.; Casado, J.; Hennrich, G.; Navarrete, J. T. L. *J. Phys. Chem. B* **2006**, *110*, 19198–19206.
- (30) Konduri, R.; Ye, H.; MacDonnell, F. M.; Serroni, S.; Campagna, S.; Rajeshwar, K. *Angew. Chem., Int. Ed.* **2002**, *41*, 3185–3187.
- (31) Klán, P. *Photochemistry of Organic Compounds [Electronic Resource]: From Concepts to Practice*; Wiley: Chichester, U.K., 2009.
- (32) An impurity was observed in our MSeV²⁺ sample, the excited state decay of which ($\tau_{\text{eff}} = 108 \pm 1$ ps) was accounted for in our data analysis (Figures S13, S16)
- (33) Koziar, J. C.; Cowan, D. O. *Acc. Chem. Res.* **1978**, *11*, 334–341.
- (34) Albert, W. Z. *J. Phys. Chem.* **1982**, *1133*, 93–98.
- (35) Fukuzumi, S.; Ohkubo, K.; Suenobu, T.; Kato, K.; Fujitsuka, M.; Ito, O. *J. Am. Chem. Soc.* **2001**, *123*, 8459–8467.
- (36) El-Sayed, M. A. *J. Chem. Phys.* **1974**, *60*, 4502–4507.
- (37) An impurity was observed in our SeExBox⁺⁺ sample, the excited state decay of which ($\tau_{\text{eff}} = 197 \pm 7$ ps) was accounted for in our data analysis.
- (38) An, Z.; Zheng, C.; Tao, Y.; Chen, R.; Shi, H.; Chen, T.; Wang, Z.; Li, H.; Deng, R.; Liu, X.; Huang, W. *Nat. Mater.* **2015**, *14*, 1476–4660.
- (39) Baldo, M. A.; O'Brien, D. F.; You, Y.; Shoustikov, A.; Sibley, S.; Thompson, M. E.; Forrest, S. R. *Nature* **1998**, *395*, 151–154.
- (40) Lakowicz, J. R. *Principles of Fluorescence Spectroscopy*, 3rd ed.; Springer: New York, 2006.
- (41) Dexter, D. L. *J. Chem. Phys.* **1953**, *21*, 836–850.
- (42) Förster, T. *Ann. Phys.* **1948**, *437*, 55–75.
- (43) Chang, J. C. *J. Chem. Phys.* **1977**, *67*, 3901–3909.
- (44) Lefler, K. M.; Brown, K. E.; Salamant, W. A.; Dyar, S. M.; Knowles, K. E.; Wasielewski, M. R. *J. Phys. Chem. A* **2013**, *117*, 10333–10345.
- (45) Biedermann, F.; Elmalem, E.; Ghosh, I.; Nau, W. M.; Scherman, O. A. *Angew. Chem., Int. Ed.* **2012**, *51*, 7739–7743.
- (46) Ford, W. E.; Kamat, P. V. *J. Phys. Chem.* **1987**, *91*, 6373–6380.
- (47) Carmieli, R.; Zeidan, T. A.; Kelley, R. F.; Mi, Q.; Lewis, F. D.; Wasielewski, M. R. *J. Phys. Chem. A* **2009**, *113*, 4691–4700.
- (48) Zhao, J.; Wu, W.; Sun, J.; Guo, S. *Chem. Soc. Rev.* **2013**, *42*, 5323–5351.
- (49) Klajn, R.; Olson, M. A.; Wesson, P. J.; Fang, L.; Coskun, A.; Trabolsi, A.; Soh, S.; Stoddart, J. F.; Grzybowski, B. A. *Nat. Chem.* **2009**, *1*, 733–738.